Origami-Inspired Electret-Based Triboelectric Generator for Biomechanical and Ocean Wave Energy Harvesting

Kai Tao[a,b*], Haiping Yi[a,b], Yang Yang[b], Honglong Chang[b], Jin Wu[c*], Lihua Tang[d], Zhaoshu Yang[d], Nan Wang[e], Liangxing Hu[e], Yongqing Fu[f], Jianmin Miao[e] and Weizheng Yuan[b*]

[a]Research & Development Institute in Shenzhen, Northwestern Polytechnical University, Shenzhen 518057, PR China

[b]Ministry of Education Key Laboratory of Micro and Nano Systems for Aerospace, Northwestern Polytechnical University, Xi'an 710072, PR China

[c]State Key Laboratory of Optoelectronic Materials and Technologies, Key Laboratory of Display Material and Technology, School of Electronics and Information Technology, Sun Yat-sen University, Guangzhou 510275, PR China

[d]Department of Mechanical Engineering, University of Auckland, 20 Symonds Street, Auckland 1010, New Zealand

[e]School of Mechanical and Aerospace Engineering, Nanyang Technological University, 50 Nanyang Avenue, 639798 Singapore

[f]Faculty of Engineering and Environment, Northumbria University, Newcastle upon Tyne, NE1 8ST, UK

Submitted to: Nano Energy

Corresponding author:

taokai@nwpu.edu.cn; wujin8@mail.sysu.edu.cn; yuanwz@nwpu.edu.cn

ABSTRACT

One of the critical issues for the conventional TENGs for applications in biomechanical and blue energy harvesting is to develop adaptive, simple-structured, high performance but low-cost TENGs for the complex excitation conditions. To solve this problem, we propose an origami-inspired TENG integrated with folded thin film electret, which can be facilely formed from two pieces of liquid crystal polymer (LCP) strips through high degrees of paper folding. It has been proved efficient for harvesting energy from both sinusoidal vibrations and impulse excitations which are universally existed in the ambient environment. Double-side corona discharging process is employed to maximize the charge density generated by the electret thin films. Attributing to the excellent elastic property of self-rebounding spring structures based on the origami design, the flexible TENGs can be readily integrated into smart shoes, floors, watches and clothes for wearable and energy harvesting applications. Triggered by impulse excitations of gentle finger tapping, instantaneous open-circuit voltage and short-circuit current of 1000 V and 110 μA, respectively, have been obtained with a remarkable peak power density of 0.67 mW/cm^3 (or 1.2 mW/g). A spherical floating buoy generator integrating multiple origami TENGs is further developed to harvest ocean wave energy at various frequencies and amplitudes as well as in arbitrary directions. The outcomes of this work offer new insights of realizing single structured TENG design for multifunctional applications.

KEY WORDS:

Triboelectric nanogenerator; Electret; Origami; Vibration energy harvesting; Wave energy harvesting; Multifunctional

1. INTRODUCTION

The rise of internet of things (IoT) and wearable/portable electronics has resulted in significant impacts on society in various fields such as healthcare, entertainment, personal communication, and environmental monitoring [1, 2]. Searching for cheap, portable and sustainable energy resources for these low-power electronics is of great significance to improve the quality of our daily life [3, 4]. Energy harvesting systems as self-sustained power sources are capable of capturing and transforming unused wearable and biomechanical energy into electrical energy, providing an alternative to the conventional electrochemical batteries and empowering self-autonomous devices and intelligent monitoring systems [5]. In general, kinetic energy of an object can be transformed into electrical energy through electrostatic [6], electromagnetic [7], piezoelectric [8-10], magnetostrictive [11] and triboelectric mechanisms [12-14]. Among various types of energy harvesters reported in literature, triboelectric nanogenerators (TENGs) based on coupling of triboelectricfication and electrostatic induction have demonstrated their unique advantages in terms of high energy conversion efficiency, diverse material selection and ease of fabrication [12-15].

Recently, various strategies have been proposed to improve the output performance of the TENGs, including synthesis of functional materials [16], nanostructured surface modifications of contact polymer materials [17-19], smart designs with arch-shaped plates [20-22], or optimizations of multilayered structures [23-30]. However, these approaches still encounter major challenges.

- The nanostructured surface modification of contact polymer material, with its complicated fabrication process, is unfavorable for large-scale batch-fabrication and long-term durability [19].
- The auxiliary architectures, designed to support the periodical contact and separation operations, make the whole device bulky and difficult to be integrated with wearable or biomechanical microsystems [23, 24].
- The currently used rigid designs of TENGs usually have restricted operation frequencies and directions, making them difficult to be adapted to excitation vibrations with irregular, random, and low-frequency characteristics, such as ocean waves [31-36].
- The output power of TENGs is quadratically proportional to the triboelectric surface charge density, therefore, the electrostatic induction of TENGs is severely affected by the effective surface charge density which only relies on contact triboelectrification [37]. However, the charge trapping capability of the contact material is not fully exploited.

To solve the above problems, in this paper, we propose an origami-inspired TENG with folded thin film electret which exhibits several unique advantages:

- Stacked multilayer TENGs can be readily constructed using the design of origami, the ancient Japanese art of paper folding built up from strips of paper, to create complex, flexible and deformable 3D TENGs from a 2D sheet substrate. The facile and low-cost formation process is critically applicable for future massive production.
- Owing to the effectively increased surface areas using the unique origami-multilayer structure, both the contact triboelectrification effect and capacitance variation of electrostatic induction are significantly amplified.
- To further maximize the electrostatic induction in the TENGs, a double-side corona discharging process is utilized in order to enhance the charge density in the thin film electret.

Due to the synergized merits of these two strategies, high performance of energy harvesting is achieved without using any complicated nanostructured polymer materials or causing any surface fatigue upon prolonged friction. Due to its light weight, long-term durability and excellent flexibility, this newly designed TENG can be easily integrated to wearable electronics for mechanical energy harvesting. We prove that by impulse exciting the TENG upon gently tapping using fingers, it instantaneously generates open-circuit voltage and short-circuit current of 1000 V and 110 μA, respectively, with a maximum power density of 0.67 mW/cm^3 (or 1.2 mW/g). A spherical design of TENG is further realized based on a spring-mass-damper system consisting of a center movable seismic ball suspended by six sets of origami TENG spring structures which have demonstrated to harvest the low-frequency ocean (or blue) wave energy effectively.

2. EXPERIMENTAL METHODS

Fig. 1a shows a 3D schematic illustration of proposed electret-based TENG (e-TENG) with a double-helix multilayered architecture, which can be readily constructed using the origami design, e.g., using the folding structures built up from two polymer strips. Both the strips are made from 50 μm/25 μm/50 μm thick copper/LCP/copper sandwiched composite-structures (Fig. 1b). The middle layer of LCP is a partially crystalline aromatic polyester with a low Young's modulus of 2.16 GPa but with a high tensile strength of up to 180 MPa. The LCP has excellent flexibility that can be served as bending joints of the paper strip and sustain long-term cyclic folding, bending and unfolding movements. Copper thin films are deposited on both sides of the LCP using a high-temperature tape-casting technique. To minimize the potential crack damage of the copper thin films, their thickness are maintained to be around 50 μm.

To promote contact electrification, the surface of the copper is treated using a dip-etching process to create nanostructured patterns using hydrochloric acid and ferric chloride solution. Scanning electron microscope (SEM) image shows that the surface of the copper grain size is around tens to hundreds of nanometers after 3 min dip-etching process (Fig. 1c). The copper sheets play double roles of (1) conduction electrodes for electrical connection, and (2) interfacial surfaces for contact triboelectrification. SEM image and output performance comparisons between unprocessed and processed copper surfaces can be found in the supporting information (Figures S1 and S2). Figures S3a and S3b show SEM images of top surface of LCP thin film surface and cross-section view of Cu/LCP/Cu sandwiched structure, respectively.

One of the two LCP strips is sandwiched with 50 μm thick fluorinated ethylene propylene (FEP) thin films on both sides. The FEP is terminated with the electronegative fluoro-group (which is also an excellent electret material), which performs as the negative side of the e-TENG. Figs. 1d and 1e show the images of fabricated e-TENG device at a compressed state and a stretched state, respectively. The double-helix spring origami architecture endows the TENG with excellent elastic and flexible properties, being compact, light-weight and extremely sensitive to vibration. The whole e-TENG device is capable of bouncing back from a compressed or stretched state to its original state without need of any auxiliary resilience support, making it applicable in a variety of applications, such as biomechanical, wearable and blue (ocean wave) energy harvesting.

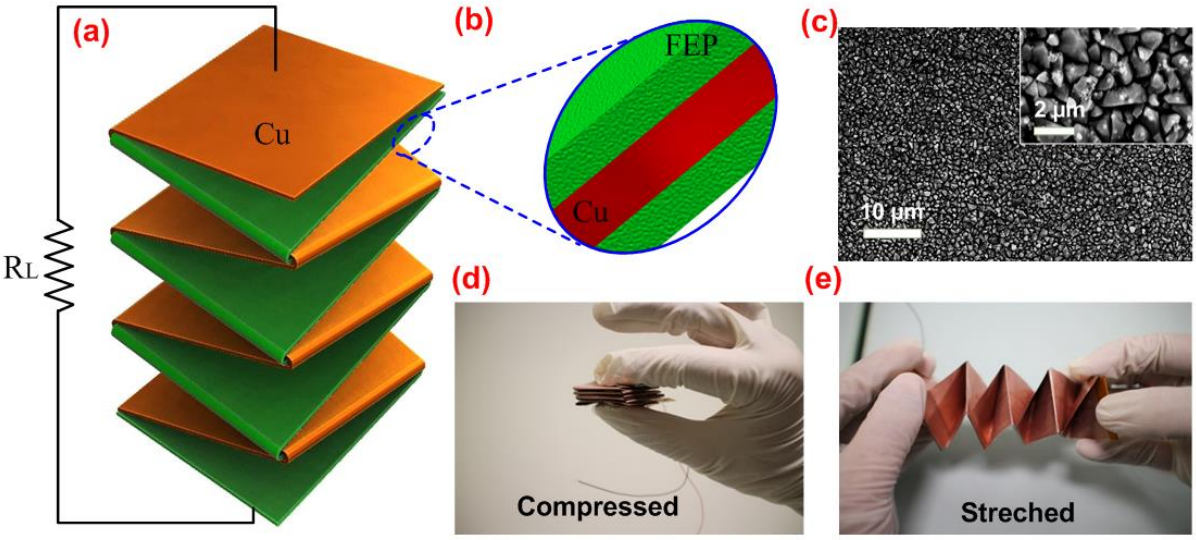

Figure 1. Illustration and images of proposed origami-inspired e-TENG: (a) Schematic configuration; (b) Enlarged cross-section view of FEP/Cu/FEP sandwiched structure; (c) SEM image of nanostructured surface of etched copper sheet. The inset is an enlarged SEM image showing the size of copper grain around hundreds of nanometers after 3 min dip-etching process. (d-e) Photographs of fabricated device at compressed state and stretched state.

Fig. 2 shows the fabrication and operating principles of the proposed origami e-TENGs. To increase the electrostatic induction during the repeated compress-release cycles, ionized charges are pre-implanted into the FEP electret thin films through a corona discharging process as a constant bias, which will be explained in details later. Electrets are dielectrics with quasi-permanent electric charges or dipole polarization, which is capable of providing a permanent electric field for years. Electret materials can be divided into two categories: SiO_2-based inorganic (SiO_2, Si_3N_4) electrets and polymer-based organic (Teflon, Parylene, FEP, PVDF, CYTOP) electrets. They are widely used in microelectromechanical systems (MEMS)such as microphones [38]. Organic electrets (such as the FEP used in the current study) are more advantageous in energy harvesting applications due to their relatively high surface charge density (up to 3.7mC/m^2 [39]), long-term stability and better flexibility.

Several major methods are usually used to implant charges into electrets, such as corona discharging [26], contact charging [40], X-ray irradiation [41], thermal poling and electron gun injection [37]. Corona discharging process is used in the current work due to its simple process and low-cost implementation as well as commercial availability. The FEP thin film electret is

firstly mounted on two sides of the Cu/LCP/Cu substrate using epoxy as a bonding layer, and then charged by the corona discharging systems based on a triode-needle-grid setup (Fig. 2a). The air surrounding the tip of needle with a high potential gradient becomes ionized and partially conductive, and is subsequently driven to the lower potential grid. Charged particles (including $CO_3^-, NO_3^-, NO_2^-, O_3^-, O_2^-$) are then uniformly implanted into the electret by the electrostatic field between the grid and substrate. The surface charges on the electret are susceptible for neutralization by the air. To improve its stability during the discharging process, multiple cycles of discharging processes with the substrate heated to a temperature of 80℃ are applied. Supplementary information provides the evidence of improved charge stability after cycling discharging process and heating process at 80℃ (Figure S4).

After both sides of the LCP-FEP are charged, the 3D TENG is finally constructed from two pieces of 2D polymer strips through high degrees of folding along predefined creases. Each time the bottom paper strip is transversely folded over the top strip till the end (Fig. 2b). Using the origami design, the complex 3D TENGs can be facilely formed with a self-suspended multilayered double-helix structure for energy harvesting.

Fig. 2c shows charge circulation within the proposed origami e-TENG in one compress-release cycle. At the initial state, the conductive electrodes and electrets are interlaced and stacked with each other (i). Electrostatic induction takes place when the stacked plates are moved towards each other under an external compressive force. At this stage, the implanted charges in the electrets play a critical role in charge circulation (ii); Triboelectrification effect occurs when the multilayered plates are pressed and intimately contacted between each other (iii); After the external force is removed, the e-TENG is restored to its original position due to the internal self-bouncing force of the multifold origami structure, thus causing the charges to flow back to its original state (iv). By this way, both electret-based electrostatic induction and contact triboelectrification are generated during the charge circulation process, thus leading to a superior charge synchronization within this unique origami-multifold structure.

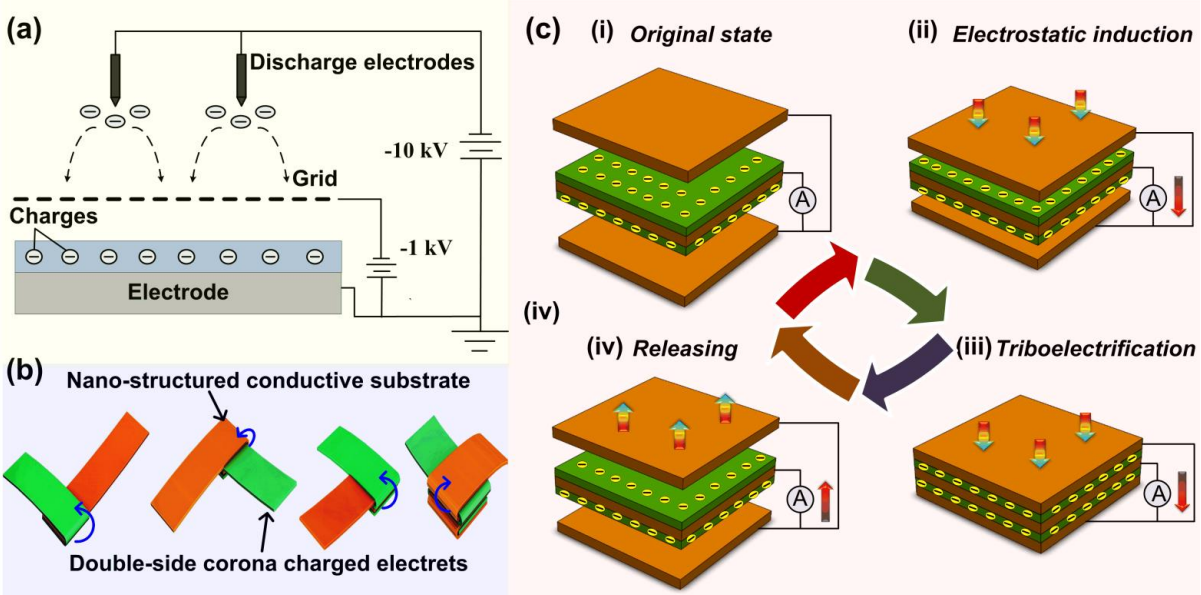

Figure 2. Fabrication and operating principles: (a) Formation and double-side corona discharging electret plates; (b) Constructing 3D origami e-TENG folded using two polymer strips; (c) Charge circulation in one compress-release cycle: (i) initial state; (ii) Electrostatic induction when electrets and copper electrodes move forward with each other under external compressive force; (iii) Triboelectrification takes place when the multilayered plates get intimate contact with each other; (iv) Charge flows back when the e-TENG rebounds back to its initial state due to its origami spring force

3. RESULTS AND DISCUSSIONS

3.1 Characterization of origami e-TENG with sinusoidal vibration

The mechanical properties of the proposed origami e-TENG are characterized usuing a linear motor (Fig. 3a). The e-TENG device is sandwiched using two parallel movable plates, whose displacement and the applied compression force can be real-time monitored. From Fig. 3a, it can be seen that the capacitance value is varied from 182 pF to 892 pF when the height of the origami structure is changed from 0.5 cm to 2.7 cm. The large capacitance variation is mainly due to compact origami structures with multilayered folded strips. For the conventional two-plate gap-closing TENGs, the capacitance can be expressed as [42]:

$$C(t) = \frac{\varepsilon_0 A}{2d/\varepsilon_1 + g - x(t)} + C_p \tag{1}$$

where A represents the overlapping area; $x(t)$ is the displacement of the movable electrodes; g and d denote the air gap and thickness of the electret thin films, respectively; ε_0 and ε_1 are the

vacuum permittivity and the dielectric constant of the electret, respectively; C_p is the parasitic capacitance, which plays an important role of the total capacitance. For multilayered origami structures, the overall capacitance can be further written as:

$$C_n(t) = \frac{(2n)^2 \varepsilon_0 A}{4nd/\varepsilon_1 + g - x(t)} + 2n \cdot C_p \tag{2}$$

where *n* is the number of layers of origami structure. If parasitic capacitance (C_p) is neglectable (which is true in this case), the overall capacitance of origami structure is increased $\sim(2n)^2$ times compared to that of the conventional two-plate TENGs. This certainly has boosted the output performance of the TENG. The illustrations of capacitance variations of two-plate and multi-plate structures are shown in the supplementary material (Figure S5).

One of the main merits of the proposed origami e-TENG is the usage of double-helix self-suspended origami spring structure, which could bounce back to its original height without any auxiliary supporting materials. Fig. 3b shows the variations of compression force as a function of out-of-plane displacement of the spring structure, which exhibits a spring hardening and nonlinear relationship. The spring stiffness of the fabricated origami structure is varied from ~24 N/m to ~96 N/m when the thickness of the origami structure is changed from 0.6 cm to 2.7 cm. The occurrence of spring hardening effect is mainly due to the large deformation of spring structure and the effective coupling of two paper strips.

Figs. 3c and 3d show magnitudes of output voltages and time-domain waveforms as a function of different excitation accelerations, respectively. With the excitation acceleration is increased from 0.1 g to 1.6 g, the output voltages are increased from 18 V to 280 V. It can be clearly observed that the output performance is quasi-linearly dependent on the excitation accelerations, which proves that the proposed origami e-TENGs have the great potential being developed as a self-powered acceleration sensor [43].

The frequency response of the origami-spring e-TENGs is further characterized by mounting the device onto an electromagnetic vibrator, which provides out-of-plane vibrations with controlled frequency and amplitude. A seismic mass of 3 g is bonded onto the top of the origami e-TENG structure. The whole set-up can be modeled as a spring-mass-damper system, which consists of a spring stiffness *k*, a seismic mass *m* and damping ratio ξ. For a sinusoidal

excitation vibration (e.g., $y = Y\sin(\omega t)$, in which y is excitation waveform , Y is amplitude, ω is frequency of the excitation and t is time), the output power of the resonant system can be derived as [44]

$$P_{W\&Y} = \frac{m\xi A'^2\omega^3(\omega/\omega_n)^3}{(1-(\frac{\omega}{\omega_n})^2)^3 + [2\xi(\frac{\omega}{\omega_n})]^2} \tag{3}$$

where ω_n is the natural frequency of spring-mass-damper system and A' is the amplitude. The maximum output power can be achieved when the natural frequency coincides with the excitation frequency. Fig. 3e shows the frequency responses of proposed e-TENG under an excitation acceleration of 1g with the frequency varied in the range of 20-50 Hz. It can be seen that the maximum output power is achieved around 25-45 Hz with broadband frequency characteristics, which are beneficial for harvesting wideband kinetic energy in the ambient environment. According to the natural frequency of a free vibration system, e.g., $f = \frac{\sqrt{k/m}}{2\pi}$, the natural frequency of the device can be estimated to be ~28 Hz. The slight deviation in the theoretical and measurement values is mainly due to the damping effects, vibration uncertainties and friction of the joint points of two polymer strips. These will affect the mechanical quality factor of the origami e-TENG. Fig. 3f shows the detection responses by dropping coins of 100 cents, 50 cents and 10 cents (RMB) onto the device from a height of 30 cm above. The precise responses according to the different dropping items clearly demonstrate its excellent sensitivity for monitoring external forces using the double-helix origami spring structure.

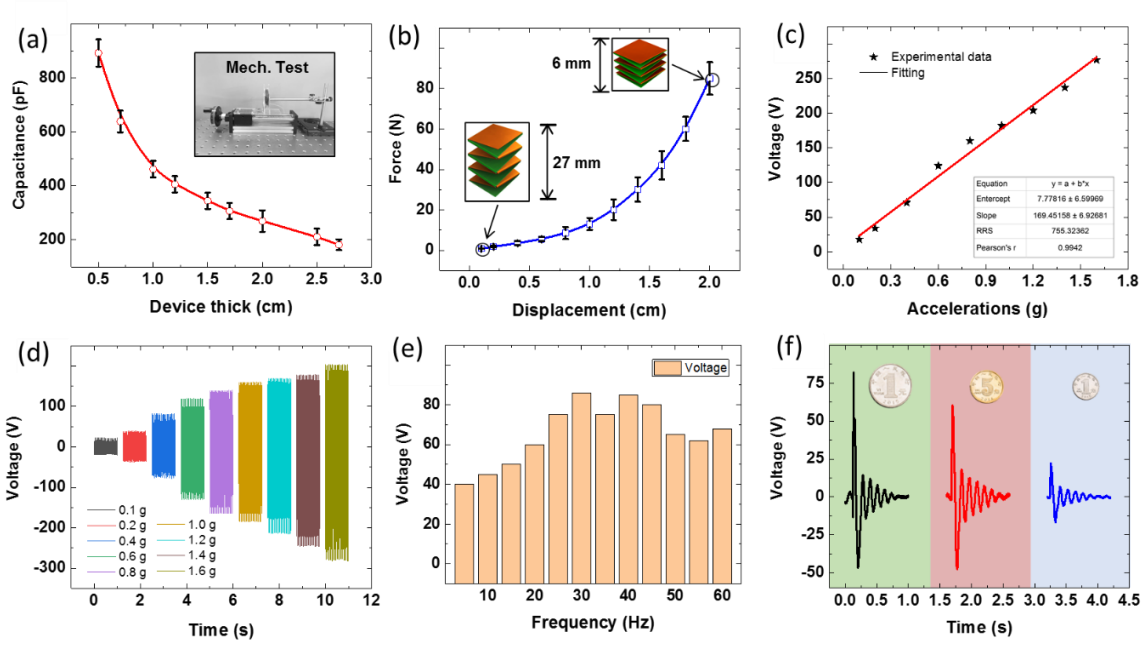

Figure 3. Mechanical characterization of proposed origami e-TENG with a linear motor: (a) Capacitance variation versus device thickness; (b) Rebound force measurement as a function of recovery displacement of the structure; (c-d) Output voltage results and time-domain voltage waveforms versus different excitation accelerations; (e) Measured frequency responses of origami e-TENG under out-of-plane vibration excitations; (d) Sensitive detection responses with dropping different coins of 100 cents, 50 cents and 10 cents onto the device from a height of 30 cm above.

The electrical properties of the devices are characterized by squeezing the origami e-TENG between two parallel plates with a load resistance of 20 MΩ (Fig. 4a). One of the plate is fixed to a 3D positioning stage, which defines the maximum movement of the origami e-TENG. The gap is varied between 0.5 cm and 2.7 cm during all the tests. The other plate is fixed onto the electromagnetic vibrator which provides a periodic compression force with a frequency of 30 Hz and an excitation acceleration of 3.8~11.4 m/s^2. The obtained time-domain output voltages and enlarged waveforms are shown in Figs. 4a and 4b, respectively. In order to be able to supply enough powers for wireless sensor nodes (WSNs) using the energy harvesting techniques, the charges generated are usually needed to be stored in a capacitor or battery as a buffer for power supply. The obtained waveform displays a proximately sinusoidal wave, which is beneficial for energy storage compared to that using the impulse signals. Fig. 4c shows the corresponding charging circuit diagram and obtained charging curves using various capacitors of 0.1 μF, 0.47 μF and 2.2 μF by cyclic compressing the e-TENG. Two switches are also used for controlling the charging process and monitoring the capacitance voltage. Clearly it is capable of charging 0.1 μF and 2.2 μF to the capacitor with the saturated voltages of 50 V and 30 V in only 2 and

120 seconds, respectively, demonstrating its effective power generation and charging applicability.

To further optimize the power generation, parametric study is conducted to investigate the output performance under different excitation conditions. Figs. 4d and 4e show 3D plot of output currents and powers under various load resistances and external excitation accelerations. It can be found that the maximum output powers of 0.21 mW, 0.87 mW and 2.7 mW are obtained at the various load resistances of 9.1 MΩ, 9.0 MΩ and 7.1 MΩ with excitation accelerations of 3.4 m/s^2, 7.8 m/s^2, 11.4 m/s^2, respectively. It should be noted that the optimum load resistances are decreased with the increase of the output power. This is because that the capacitance is gradually increased at higher excitations. For vibration energy harvesters, the optimum output power is achieved when the external load matches the internal impedance of generator [45]. Therefore, a larger capacitance variation will result in a lower optimum impedance for the proposed origami e-TENG according to impedance expression $R \propto \frac{1}{j\omega C}$ [45], where ω and C are the frequency and capacitance, respectively. Fig. 4f depicts the output voltages versus different gap distances in 0.5~2.7 cm and accelerations in 3.8~11.4 m/s^2. An optimum output voltage is achieved when the gap of two plates is within 0.8~1.2 cm, regardless of excitation conditions.

Figure S6 show output voltages and powers of the e-TENG with an area of 3 × 3 cm^2 at a load resistance of 105MΩ and an acceleration of 7.6m/s^2 with different origami layers: e.g., one layer, two layers and three layers. Figure S7 shows the output voltages and powers of the e-TENG with three origami layers at a load resistance of 105 MΩ and an acceleration of 7.6 m/s^2 with different electrode areas: e.g., 1 × 1 cm^2, 2 × 2 cm^2, 3 × 3 cm^2. It can be seen that the output performance is enhanced with the increase of the foldable layers and surface areas. The maximum output performance is achieved from the three-layer origami structure with an area of 3 × 3 cm^2.

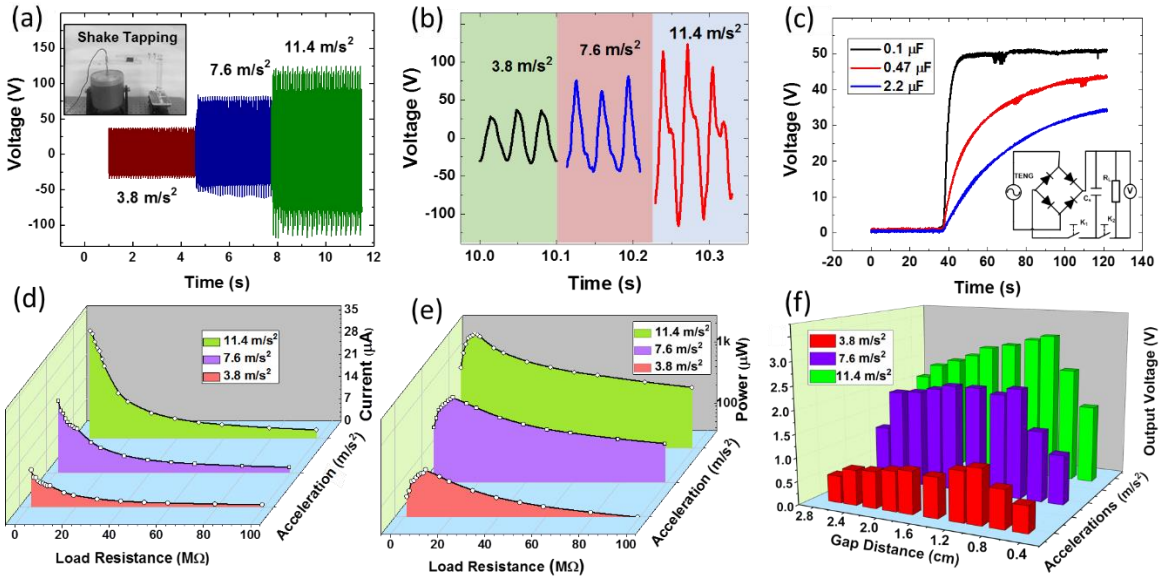

Figure 4. Electrical characterization of proposed origami e-TENG under periodic compressive force provided by a shaker at 30 Hz and accelerations of 3.8~11.4 m/s^2: (a-b) Time-domain output voltages and enlarged waveforms; (c) Schematic illustrations of full-wave rectifier charging circuit and typical capacitor charging curves of 0.1, 0.47 & 2.2 μF; (d-e) Output currents and power optimizations under various load resistances and external excitations; (f) Output voltage optimizations with different gap distances in 0.5~2.7 cm and accelerations in 3.8~11.4 m/s^2

3.2 Characterization of origami e-TENG with impulse excitation

One of the main potential applications for the proposed origami e-TENGs is for wearable devices having the characteristics of low-frequency and intermittent impact excitations. Therefore, the origami e-TENG is put on the desk and tapped simply using the finger at different tapping frequencies. Figs. 5a and 5b show the obtained open-circuit voltages and waveforms during the finger tapping tests. It can be seen that the peak-to-peak open-circuit voltage is up to 1004 V with a small device volume of 16.7 cm^3 and a weight of 9.3 gram. Due to its self-bouncing nature, the TENG is capable of continuously vibrating for nearly 2 seconds in a free vibration condition as can be seen from the electrical signals shown in Fig. 5b. The instantaneous maximum output power of 11.2 mW is obtained with an optimum load resistance of 6.28 MΩ (Fig. 5c), corresponding to a high volume power density and weight power density of 0.67 mW/cm^3 and 1.2 mW/g, respectively. The instantaneous short-circuit current can be as high as 110 μA under different tapping frequencies (Fig. 5d). Supplement material Video S1 demonstrates that 120 numbers of LED bulbs can be lightened up by simple and gentle finger tapping on the TENG device. This represents one of the highest performance micro-electret

harvesters reported so far.

In order to study the charge stability of proposed origami e-TENG device, we continuously monitor the surface potential of FEP electrets within a period of 90 days after corona discharging process. As shown in Fig.5e, the surface potential decreases rapidly within the first a few days, but then becomes nearly stabilized, and still maintains about 74% of its initial potential after 90 days. When the origami e-TENG is continuously compressed using the shaker tapping process, the generated output voltages only show minor decreases after 144,000 contact-release cycles (Fig. 5f). These two types of measurements clearly demonstrated the enhanced performance and long-term stability of corona-charged FEP electrets.

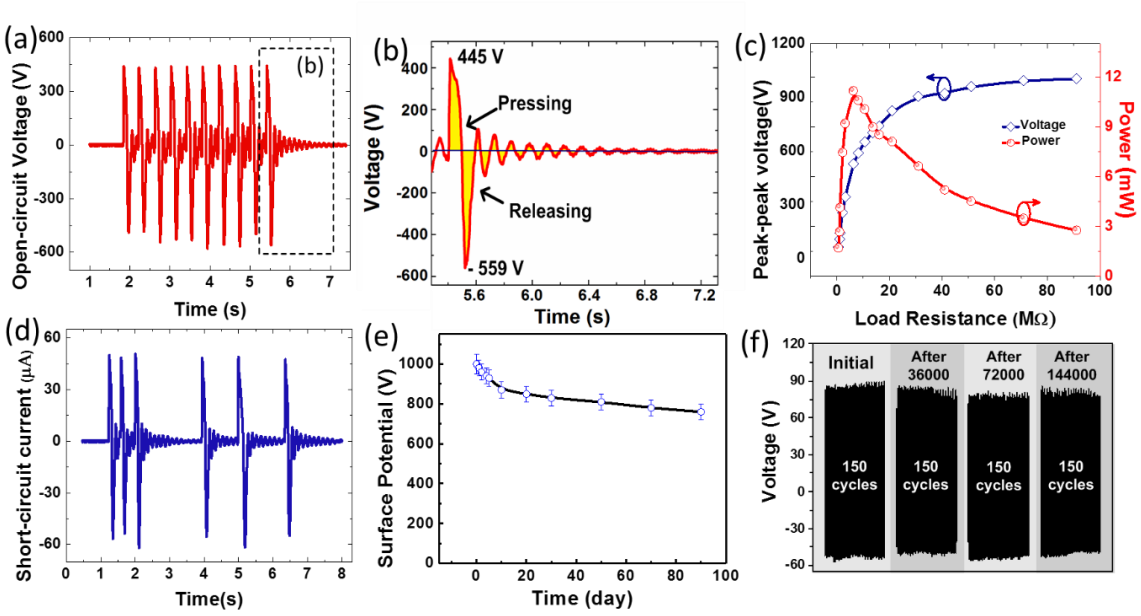

Figure 5. Finger tapping characterizations of proposed origami e-TENG: (a) Peak-to-peak open-circuit output voltages up to 1000 V; (b) Enlarged view of output voltage waveforms in pressing and releasing process; (c) Maximum output power of 11.2 mW obtained at optimum load resistance of 6.28 MΩ; (d) Peak short-circuit current of 110 μA at different tapping frequencies; (e) Stability characterization of e-TENG surface potential on the FEP layer in 90 days after corona discharging process; (f) Output performance stability of e-TENG after continuously operating ~144000 cycles

3.3 Wearable applications of origami e-TENG

The origami e-TENG is convenient to be integrated with wearable electronics due to its lightweight, low cost, simple structure and small size. Fig. 6 demonstrates the applications of

origami e-TENGs in applications of biomechanical energy harvesting and self-powered human-motion monitoring. The flexible e-TENG is found to be sensitive to small changes in the mechanical force. Figs. 6(a) to 6(d) show the origami e-TENG has been used for monitoring elbow bending, arm swinging, finger motion and knee bending movements. It can be seen that the respones of the device is very fast when the joint moves in different angles or different ampltiudes.

Figs. 6(e) to 6(g) show the snapshots of demonstration images for biomechanical energy harvesting process by connecting hundreds of LEDs in serials. The tiny origami e-TENG can be installed at the backside of a watch for energy harvesting process (see Fig. 6(e), Video S2). When there is a relative movement between the watch and wrist, for example, during hand shaking, the compression or stretching forces would be easily converted into electrical power using the designed TENG device. The flexible TENG can also be integrated within the shoes without sacrificing any comfortability due to its smaller size (see Fig. 6(f), Video S3). It is also capable of lighting hundreds of LEDs when a person is walking with the shoe.

Due to its high flexibility and durability, the TENG can also be integrated within clothes (see Fig. 6(g), Video S4). Simiarly hunderds of LEDs can also be lighted up when the arm with the TENG installed is swinging up and down or coats wobbling. It should be noted that since the full-wave rectifier circuit is used during the demonstration, the On/Off times of the LED array is longer than the motion frequency. Due to its facile and low-cost fabrication process, an array of origami e-TENGs are easily installed beneath the ground of a smart floor for converting footsteps into electrical power and geneating useful data information. Supplemental materials (e.g., Figure S8a and S8b) show the schematic and the fabricated prototype of smart floors integrated with 16 origami structures inside. Video S5 demonstrates that the floor with the TENGs can sustain and collect energy upon generating different types of human motions, including stepping and jumping. It is expected that the designed smart floors can be easily installed in streets, retail and transport hubs, where there are much higher chances of movements of people. The converted power has potential applications in green energy generation, transportation monitoring and big data analysis for future smart cites.

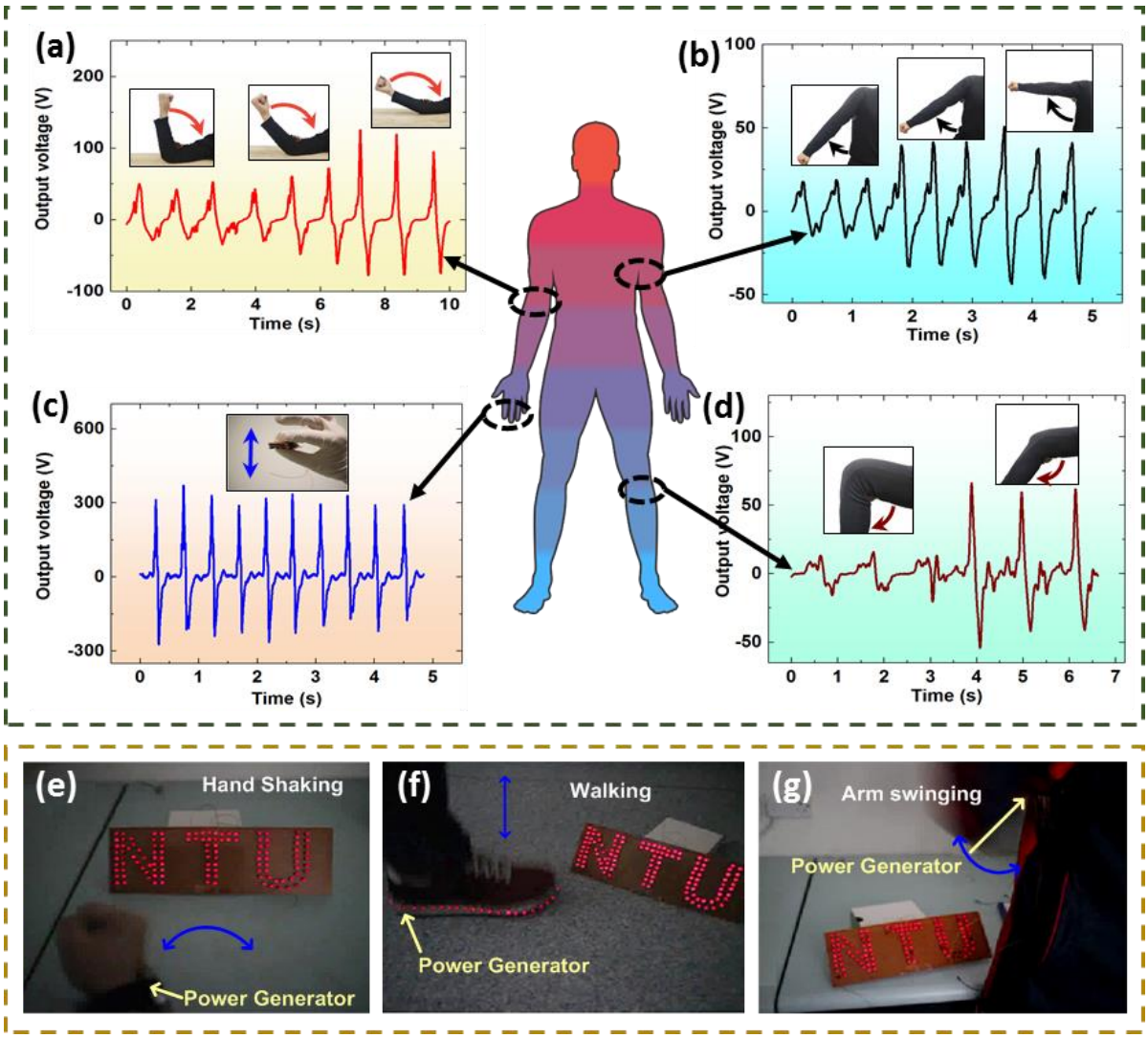

Figure 6. Origami e-TENGs for wearable energy harvesting and as self-powered motion monitoring: (a) Elbow bending movement at 90°, 120° and 150°; (b) Arm swinging movement at 30°, 60° and 90°; (c) Hand squeezing of origami-TENG; (d) Knee bending movement at 90°, 120° and 150°; (e-g) Snapshots of power generation demonstration by serial connections of hundreds of LEDs with hand shaking, walking and arm swinging

3.4 Ocean wave energy harvesting of the origami e-TENG

Ocean covers over 70% surface of our planet, and ocean (or blue) waves are considered as high power density and widely distributed energy sources in the ambient environment [46-48]. The ocean waves have the unique dynamic characteristics of irregular and random vibrations with mixed amplitudes and frequencies [31-36]. Herein, we proposed to use our developed TENGs to fabricate a spherical floating buoy device with integrated origami multifold electrets for ocean wave energy harvesting applications (Fig. 7). It consists of a center movable seismic ball suspended by surrounding six sets of origami spring structures. The arrays of origami e-TENGs

not only act as power generation units for converting center mass movement to electrical energy but also function as suspended spring fixtures to confine the seismic mass.

This design has several key merits. Firstly, the origami energy conversion units are evenly distributed in every direction of the spherical e-TENGs, making it capable of harvesting low-frequency kinetic energy in arbitrary directions. When the center movable seismic ball is oscillated in the sphere due to wave excitations, at least two origami units are active for energy generation. One is operated in a compression mode, whereas the other is in a stretching mode. Secondly, the light-weight and compact architecture facilitates the whole sphere devices floated on the surface of sea water. Thirdly, the overall power generation system are sealed hermetically inside the sphere, avoiding harsh environmental conditions of the sea, such as saline sea water and strong thermal irradiation. Furthermore, due to its light weight, long-term durability and excellent adaptability, the sphere floating generator can be operated in a single unit or be easily integrated into a network of TENG devices for large-scale blue energy harvesting in the sea (Fig. 7a).

Figs. 7b and 7c show the schematic and a digital photograph of the fabricated spherical floating buoy TENG in the water tank, respectively. The sinusoidal mechanical waves are generated using an acrylate plate, which is fixed onto a linear motor and controlled by a function generator with predefined frequencies of 1~3 Hz. Figs. 7d and 7e show the instantaneous output voltages and powers at various frequencies and load resistances. It can be found that an optimum output power of 55.4 μW is obtained at wave excitation frequency of 2 Hz and load resistance of 60 MΩ at small wave amplitudes. The LEDs connected to the TENGs can be instantly lightened up with a wave excitation frequency of 2 Hz (Video S6). The rectified output voltage waveform of this developed spherical TENG with a wave frequency of 2 Hz and a load resistance of 120 MΩ is depicted in Fig. 7f. The generated power is capable of charging 10 μF capacitor to 2.5 V within 60 seconds (Fig. 7g). The generated energy or power is large enough to provide powers for a series temperature and humidity sensors. The spherical e-TENG can also respond to arbitrary excitation directions. Fig. 7h shows that the maximum output power of 18.8 mW is obtained at an optimum load resistance of 3 MΩ by hand shaking. The full-wave rectified output voltage waveforms at frequency of 2 Hz are shown in Fig. 7i.

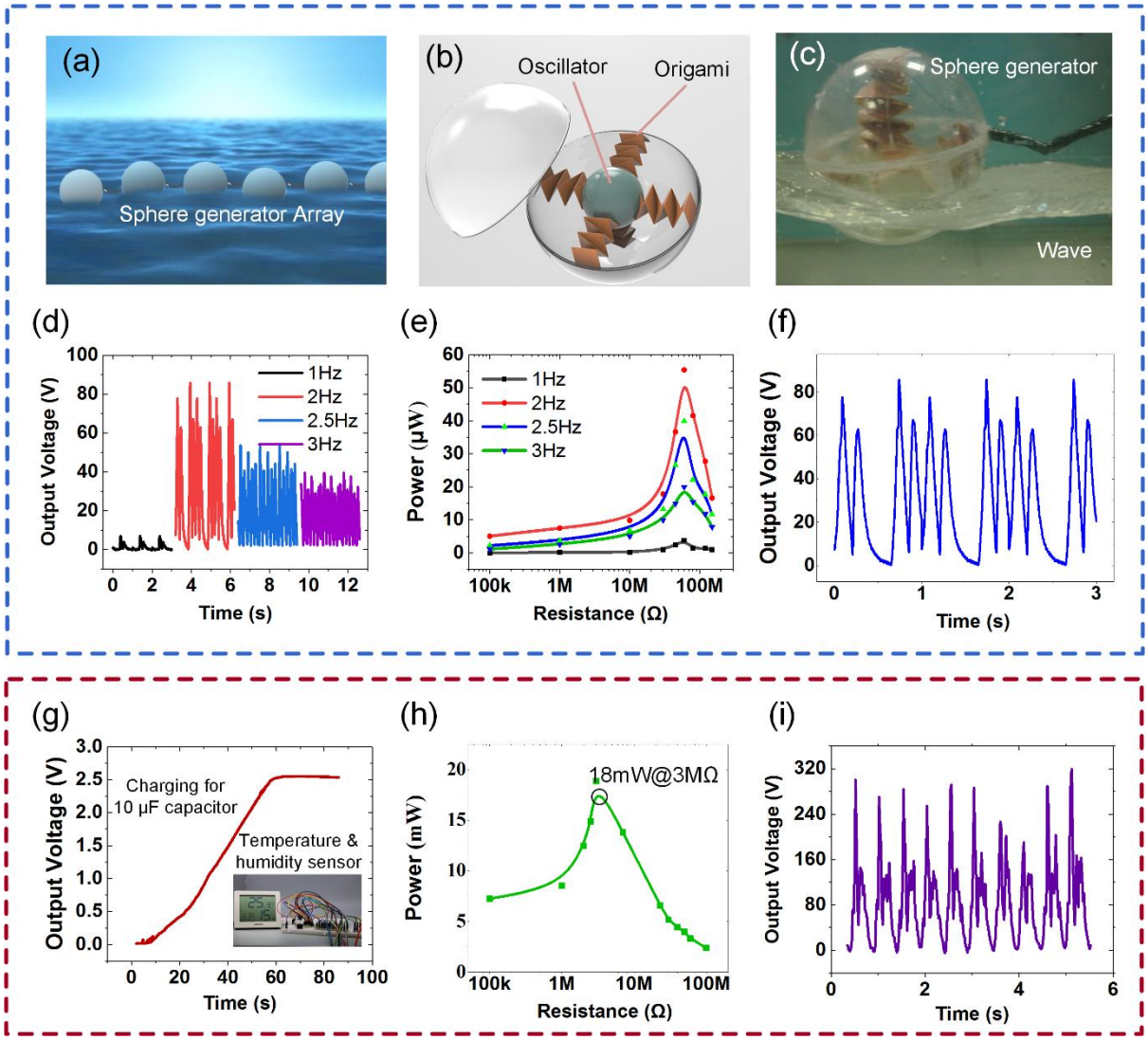

Figure 7. Spherical floating buoy TENGs for water wave energy harvesting applications: (a) Perspective of an array of spherical floating buoy TENGs; (b) A schematic illustration of spherical TENGs consisting of center movable seismic ball suspended by six sets of origami e-TENG spring structure around; (c) Digital photographs of spherical TENGs in water tank; (d-e) Output voltages and power optimizations versus different load resistances and wave frequencies; (f) Full-wave rectified output voltage waveforms at wave frequency of 2 Hz; (g) Charging curves of 10 μF capacitor by wave power generation and powering for temperature and humidity sensors; (g) Maximum output power of 18.8 mW at optimum load resistance of 3 MΩ by hand shaking the spherical TENGs ; (i) Full-wave rectified output voltage waveforms by hand shaking at 2 Hz

4. CONCLUSIONS

In summary, an origami-inspired TENG integrated with folded thin film electret was designed and prototyped, which has demonstrated the great potentials for biomechanical and ocean wave

energy harvesting. The double-helix-spring origami architecture endows proposed TENGs with excellent elastic and self-rebounding properties without any auxiliary resilient supports, making the whole device compact, light-weight and extreme sensitive. With the superior charge synchronization by the unique origami-multifold structure and double-side corona discharging process, contact triboelectrification and electrostatic induction are significantly enhanced. Mechanical, electrical and wearable properties with impulse excitation and continuous sinusoidal vibrations have been investigated comprehensively. For impulse signal by gentle finger tapping, the instantaneous open-circuit voltage and short-circuit current of 1000 V and 110 μA have been obtained, corresponding to peak power density of 0.67 mW/cm^3 and 1.2 mW/g, respectively.

Thanks to its light weight, long-term durability and excellent flexibility, the proposed origami-inspired TENG have been successfully demonstrated for wide wearable applications in smart shoes, watches and clothes, to name a few. Smart floor integrating an array of origami TENGs shows the great potential for various energy harvesting applications for future smart cities. A floating sphere generator integrating multiple TENGs is further developed which is capable of harvesting ocean wave energy from various frequencies and amplitudes in random directions, demonstrating its great potential in large-scale ocean or blue energy harvesting. This work successfully demonstrates the versatility and viability of single TENG structure for broad real-world application scenarios.

ACKNOWLEDGEMENTS

This research is supported by National Natural Science Foundation of China Grant No. 51705429, National Natural Science Foundation of Shaanxi Province No. 2018JQ5030, the Fundamental Research Funds for the Central Universities No. 31020190503003, Laboratory fund of Science and Technology on Micro-system Laboratory No. 614280401010417, Science, Technology and Innovation Commission of Shenzhen Municipality JCYJ20170815161054349, Space Science and Technology Foundation, UK Engineering and Physical Sciences Research Council (EPSRC) for support under grant EP/P018998/1, Newton Mobility Grant (IE161019) through Royal Society and the National Natural Science Foundation of China.

REFERENCES

[1] Z. L. Wang, "Nanogenerators, self-powered systems, blue energy, piezotronics and

piezo-phototronics – A recall on the original thoughts for coining these fields," no. 54 pp. 477-483, 2018.

[2] Z. L. Wang, "Triboelectric nanogenerators as new energy technology and self-powered sensors–Principles, problems and perspectives," *Faraday discussions,* vol. 176, pp. 447-458, 2015.

[3] X. Wang, L. Dong, H. Zhang, R. Yu, C. Pan, and Z. L. Wang, "Recent progress in electronic skin," *Advanced Science,* vol. 2, no. 10, p. 1500169, 2015.

[4] F. R. Fan, W. Tang, and Z. L. Wang, "Flexible Nanogenerators for Energy Harvesting and Self‐Powered Electronics," *Advanced Materials,* 2016.

[5] X. Cheng, W. Tang, Y. Song, H. Chen, H. Zhang, and Z. L. Wang, "Power management and effective energy storage of pulsed output from triboelectric nanogenerator," *Nano Energy,* 2019.

[6] F. U. Khan and M. U. Qadir, "State-of-the-art in vibration-based electrostatic energy harvesting," *Journal of Micromechanics and Microengineering,* vol. 26, no. 10, p. 103001, 2016.

[7] Y. Tan, Y. Dong, and X. Wang, "Review of MEMS electromagnetic vibration energy harvester," *Journal of Microelectromechanical Systems,* vol. 26, no. 1, pp. 1-16, 2016.

[8] Z. L. Wang and J. Song, "Piezoelectric nanogenerators based on zinc oxide nanowire arrays," *Science,* vol. 312, no. 5771, pp. 242-246, 2006.

[9] X. Wang, J. Song, J. Liu, and Z. L. Wang, "Direct-current nanogenerator driven by ultrasonic waves," *Science,* vol. 316, no. 5821, pp. 102-105, 2007.

[10] C. Pan, J. Zhai, and Z. L. Wang, "Piezotronics and Piezo-phototronics of Third Generation Semiconductor Nanowires," *Chemical reviews,* 2019.

[11] T. Ueno, "Performance of improved magnetostrictive vibrational power generator, simple and high power output for practical applications," *Journal of applied physics,* vol. 117, no. 17, p. 17A740, 2015.

[12] A. C. W. Zhong Lin Wang, "On the origin of contact-electrification," *Materials Today,* 2019 Online.

[13] H. Zou, Y. Zhang, L. Guo, P. Wang, X. He, G. Dai, H. Zheng, C. Chen, A. C. Wang, C. Xu, and Z. Wang, "Quantifying the triboelectric series," *Nature communications,* vol. 10, no. 1, p. 1427, 2019.

[14] P. Wang, L. Pan, J. Wang, M. Xu, G. Dai, H. Zou, K. Dong, and Z. L. Wang, "An Ultra-Low-Friction Triboelectric-Electromagnetic Hybrid Nanogenerator for Rotation Energy Harvesting and Self-Powered Wind Speed Sensor," *ACS Nano,* vol. 12, no. 9, pp. 9433-9440, Sep 25 2018.

[15] Z. L. Wang, J. Chen, and L. Lin, "Progress in triboelectric nanogenerators as a new energy technology and self-powered sensors," *Energy & Environmental Science,* vol. 8, no. 8, pp. 2250-2282, 2015.

[16] X. Xia, J. Chen, H. Guo, G. Liu, D. Wei, Y. Xi, X. Wang, and C. Hu, "Embedding variable micro-capacitors in polydimethylsiloxane for enhancing output power of triboelectric nanogenerator," *Nano Research,* vol. 10, no. 1, pp. 320-330, 2017.

[17] Y. Feng, Y. Zheng, Z. U. Rahman, D. Wang, F. Zhou, and W. Liu, "based triboelectric nanogenerators and their application in self-powered anticorrosion and antifouling,"

Journal of Materials Chemistry A, vol. 4, no. 46, pp. 18022-18030, 2016.

[18] H. Guo, J. Chen, Q. Leng, Y. Xi, M. Wang, X. He, and C. Hu, "Spiral-interdigital-electrode-based multifunctional device: Dual-functional triboelectric generator and dual-functional self-powered sensor," *Nano Energy,* vol. 12, pp. 626-635, 2015.

[19] X. Cheng, Z. Song, L. Miao, H. Guo, Z. Su, Y. Song, and H.-X. Zhang, "Wide range fabrication of wrinkle patterns for maximizing surface charge density of a triboelectric nanogenerator," *Journal of Microelectromechanical Systems,* vol. 27, no. 1, pp. 106-112, 2017.

[20] W.-S. Jung, M.-G. Kang, H. G. Moon, S.-H. Baek, S.-J. Yoon, Z.-L. Wang, S.-W. Kim, and C.-Y. Kang, "High output piezo/triboelectric hybrid generator," *Scientific reports,* vol. 5, p. 9309, 2015.

[21] X.-S. Zhang, M.-D. Han, R.-X. Wang, F.-Y. Zhu, Z.-H. Li, W. Wang, and H.-X. Zhang, "Frequency-multiplication high-output triboelectric nanogenerator for sustainably powering biomedical microsystems," *Nano letters,* vol. 13, no. 3, pp. 1168-1172, 2013.

[22] W. Tang, Tian, J., Zheng, Q., Yan, L., Wang, J., Li, Z., & Wang, Z. L., " Implantable self-powered low-level laser cure system for mouse embryonic osteoblasts' proliferation and differentiation," *ACS nano,* vol. 9, no. 8, pp. 7867-7873, 2015.

[23] W. Yang, J. Chen, Q. Jing, J. Yang, X. Wen, Y. Su, G. Zhu, P. Bai, and Z. L. Wang, "3D stack integrated triboelectric nanogenerator for harvesting vibration energy," *Advanced Functional Materials,* vol. 24, no. 26, pp. 4090-4096, 2014.

[24] J. Wang, Z. Wen, Y. Zi, P. Zhou, J. Lin, H. Guo, Y. Xu, and Z. L. Wang, "All‐plastic‐materials based self‐charging power system composed of triboelectric nanogenerators and supercapacitors," *Advanced Functional Materials,* vol. 26, no. 7, pp. 1070-1076, 2016.

[25] P. Bai, G. Zhu, Z.-H. Lin, Q. Jing, J. Chen, G. Zhang, J. Ma, and Z. L. Wang, "Integrated multilayered triboelectric nanogenerator for harvesting biomechanical energy from human motions," *ACS nano,* vol. 7, no. 4, pp. 3713-3719, 2013.

[26] T. Zhou, L. Zhang, F. Xue, W. Tang, C. Zhang, and Z. L. Wang, "Multilayered electret films based triboelectric nanogenerator," *Nano Research,* vol. 9, no. 5, pp. 1442-1451, 2016.

[27] L. Gao, D. Hu, M. Qi, J. Gong, H. Zhou, X. Chen, J. Chen, J. Cai, L. Wu, and N. Hu, "A double-helix-structured triboelectric nanogenerator enhanced with positive charge traps for self-powered temperature sensing and smart-home control systems," *Nanoscale,* vol. 10, no. 42, pp. 19781-19790, 2018.

[28] L. M. Zhang, C. B. Han, T. Jiang, T. Zhou, X. H. Li, C. Zhang, and Z. L. Wang, "Multilayer wavy-structured robust triboelectric nanogenerator for harvesting water wave energy," *Nano Energy,* vol. 22, pp. 87-94, 2016.

[29] X. Wang, S. Niu, F. Yi, Y. Yin, C. Hao, K. Dai, Y. Zhang, Z. You, and Z. L. Wang, "Harvesting ambient vibration energy over a wide frequency range for self-powered electronics," *ACS nano,* vol. 11, no. 2, pp. 1728-1735, 2017.

[30] M. Xu, P. Wang, Y. C. Wang, S. L. Zhang, A. C. Wang, C. Zhang, Z. Wang, X. Pan, and Z. L. Wang, "A soft and robust spring based triboelectric nanogenerator for harvesting arbitrary directional vibration energy and self‐powered vibration sensing," *Advanced Energy Materials,* vol. 8, no. 9, p. 1702432, 2018.

[31] S. L. Zhang, M. Xu, C. Zhang, Y.-C. Wang, H. Zou, X. He, Z. Wang, and Z. L. Wang, "Rationally designed sea snake structure based triboelectric nanogenerators for effectively and efficiently harvesting ocean wave energy with minimized water screening effect," *Nano Energy,* vol. 48, pp. 421-429, 2018.

[32] T. Jiang, Y. Yao, L. Xu, L. Zhang, T. Xiao, and Z. L. Wang, "Spring-assisted triboelectric nanogenerator for efficiently harvesting water wave energy," *Nano Energy,* vol. 31, pp. 560-567, 2017.

[33] D. Y. Kim, H. S. Kim, D. S. Kong, M. Choi, H. B. Kim, J.-H. Lee, G. Murillo, M. Lee, S. S. Kim, and J. H. Jung, "Floating buoy-based triboelectric nanogenerator for an effective vibrational energy harvesting from irregular and random water waves in wild sea," *Nano Energy,* vol. 45, pp. 247-254, 2018.

[34] J. Wang, L. Pan, H. Guo, B. Zhang, R. Zhang, Z. Wu, C. Wu, L. Yang, R. Liao, and Z. L. Wang, "Rational Structure Optimized Hybrid Nanogenerator for Highly Efficient Water Wave Energy Harvesting," *Advanced Energy Materials,* vol. 9, no. 8, p. 1802892, 2019.

[35] M. Xu, T. Zhao, C. Wang, S. L. Zhang, Z. Li, X. Pan, and Z. L. Wang, "High power density tower-like triboelectric nanogenerator for harvesting arbitrary directional water wave energy," *ACS nano,* vol. 13, no. 2, pp. 1932-1939, 2019.

[36] Z. Wu, H. Guo, W. Ding, Y.-C. Wang, L. Zhang, and Z. L. Wang, "A Hybridized Triboelectric–Electromagnetic Water Wave Energy Harvester Based on a Magnetic Sphere," *ACS nano,* vol. 13, no. 2, pp. 2349-2356, 2019.

[37] S. Wang, Y. Xie, S. Niu, L. Lin, C. Liu, Y. S. Zhou, and Z. L. Wang, "Maximum surface charge density for triboelectric nanogenerators achieved by ionized-air injection: methodology and theoretical understanding," *Adv Mater,* vol. 26, no. 39, pp. 6720-8, Oct 22 2014.

[38] A. G. P. Kottapalli, K. Tao, D. Sengupta, and M. S. Triantafyllou, *Self-Powered and Soft Polymer MEMS/NEMS Devices*. Springer, 2019.

[39] H.-w. Lo and Y.-C. Tai, "Parylene-based electret power generators," *Journal of Micromechanics and Microengineering,* vol. 18, no. 10, p. 104006, 2008.

[40] S. Lin, L. Xu, L. Zhu, X. Chen, and Z. L. Wang, "Electron Transfer in Nanoscale Contact Electrification: Photon Excitation Effect," *Advanced Materials,* p. 1901418, 2019.

[41] Y. Feng, K. Hagiwara, Y. Iguchi, and Y. Suzuki, "Trench-filled cellular parylene electret for piezoelectric transducer," *Applied Physics Letters,* vol. 100, no. 26, Jun 2012.

[42] K. Tao, S. W. Lye, J. Miao, L. Tang, and X. Hu, "Out-of-plane electret-based MEMS energy harvester with the combined nonlinear effect from electrostatic force and a mechanical elastic stopper," *Journal of Micromechanics and Microengineering,* vol. 25, no. 10, p. 104014, 2015.

[43] H. Chen, Y. Song, X. Cheng, and H. Zhang, "Self-powered electronic skin based on the triboelectric generator," *Nano energy,* vol. 56, pp. 252-268, 2019.

[44] C. B. Williams and R. B. Yates, "Analysis of a micro-electric generator for microsystems," *Sensors and Actuators a-Physical,* vol. 52, no. 1-3, pp. 8-11, Mar-Apr 1996.

[45] K. Tao, L. Tang, J. Wu, S. W. Lye, H. Chang, and J. Miao, "Investigation of multimodal

electret-based MEMS energy harvester with impact-induced nonlinearity," *Journal of Microelectromechanical Systems,* vol. 27, no. 2, pp. 276-288, 2018.

[46] J. An, Z. M. Wang, T. Jiang, X. Liang, and Z. L. Wang, "Whirling‐Folded Triboelectric Nanogenerator with High Average Power for Water Wave Energy Harvesting," *Advanced Functional Materials,* p. 1904867, 2019.

[47] Z. Lin, B. Zhang, H. Guo, Z. Wu, H. Zou, J. Yang, and Z. L. Wang, "Super-robust and frequency-multiplied triboelectric nanogenerator for efficient harvesting water and wind energy," *Nano Energy,* p. 103908, 2019.

[48] G. Liu, H. Guo, S. Xu, C. Hu, and Z. L. Wang, "Oblate Spheroidal Triboelectric Nanogenerator for All‐Weather Blue Energy Harvesting," *Advanced Energy Materials,* p. 1900801, 2019.